SERI/TP-217-3505
UC Category: 261
DE89009443

Three-Dimensional Airfoil Performance Measurements on a Rotating Wing

C. P. Butterfield

Prepared for the
European Wind Energy
Conference and Exposition
Glasgow, Scotland
10-13 July 1989

Prepared under Task No. WE911001

Solar Energy Research Institute
A Division of Midwest Research Institute

1617 Cole Boulevard
Golden, Colorado 80401-3393

Prepared for the
U.S. Department of Energy
Contract No. DE-AC02-83CH10093

NOTICE

Printed in the United States of America
Available from:
National Technical Information Service
U.S. Department of Commerce
5285 Port Royal Road
Springfield, VA 22161

Price: Microfiche A01
Printed Copy A02

Codes are used for pricing all publications. The code is determined by the number of pages in the publication. Information pertaining to the pricing codes can be found in the current issue of the following publications which are generally available in most libraries: *Energy Research Abstracts (ERA)*; *Government Reports Announcements* and Index (*GRA* and I); *Scientific and Technical Abstract Reports (STAR)*; and publication NTIS-PR-360 available from NTIS at the above address.

THREE-DIMENSIONAL AIRFOIL PERFORMANCE MEASUREMENTS ON A ROTATING WING

C. P. (Sandy) Butterfield

Solar Energy Research Institute, Golden, Colorado, USA

ABSTRACT

The objective of this comprehensive research program was to study the effects of horizontal- is wind turbine (HAWT) blade rotation on aerodynamic behavior below, near, and beyond stall. This paper describes the flow angle sensor used to measure angle of attack (AOA) and how the sensor was calibrated, and it gives results of pressure integrations on the blade. Aerodynamic, load, flow-visualization, and inflow measurements were made on a 10-m, three-bladed, downwind HAWT. A video camera was mounted on the rotor to record video images of tufts attached to the low-pressure side of a constant-chord, zero-twist blade. Load measurements were made using strain gages mounted every 10% of the blade's span, and pressure measurements were made at 80% of the blade's span. Pressure taps were located at 32 chordwise positions and revealed pressure distributions comparable with wind tunnel data. Inflow was measured using a vertical-plane array of eight propvane and five triaxial (U-V-W) prop-type anemometers located 10 m upwind in the predominant wind direction.

Results show evidence of stall hysteresis and unsteadiness at high AOA. Correlations with analytical predictions and wind tunnel tests show good agreement at low AOA and poor agreement at high AOA.

INTRODUCTION

Most wind turbines experience aerodynamic stall during normal operating conditions over small and sometimes large portions of the blade. The majority of HAWTs use stall to regulate peak power and loads. The operation of airfoils in and beyond stall has led to several problems. First, there is very little wind tunnel data for airfoil performance beyond the m imum lift coefficient a_x). Because wind turbines commonly operate at very AOA (30°), this leads to guessing the airfoil's performance between 12° and 30°. Beyond 30°, flat-plate theory can be used. Performance and loads predictions are based on this uncertain airfoil performance data, which contributes to significant errors in estimates of peak performance.

Secondly, the stall performance of an airfoil used on a rotating wing (such as that on a HAWT) appears to be modified by three-dimensional flow effects. It is common for wind turbine designers to underestimate peak performance and loads. Part of the cause is poor airfoil data, as mentioned above; but there is an additional effect caused by blade rotation. The lift curve slope and C_{lmax} appear to be reduced on outboard blade sections, while inboard C_{lmax} appears to be increased according to Madsen et al. (1). To understand the physics controlling this phenomenon, detailed airfoil performance measurements must be studied on a rotating wing.

Because stall is such an important issue for predicting both steady and unsteady loads, the Solar Energy Research Institute (SERI), sponsored by the United States Department of Energy, has begun a detailed measurement program on a 10-m, 3-bladed HAWT. This test has produced measurements of (1) far-field atmospheric boundary layer, (2) near-field inflow using a vertical-plane array and high-frequency response anemometry, (3) airfoil pressure distributions at 80% radius, (4) video images of surface flow patterns, (5) blade loads at nine spanwise locations, and (6) turbine structural loads. This detailed data set is being used to understand how turbulent inflow affects unsteady aerodynamics, fatigue loads, and yawed operation loads. This paper focuses only on rotating-wing aerodynamic pressure measurements.

TEST SETUP

The test program used a 10-m-diameter, three-bladed, downwind turbine with pitch control. A constant, 45-cm-chord blade was used with an S809 airfoil [Tangler (2)] The details of the overall test setup are covered by Butterfield (3). This paper addresses only the details of the pressure-measuring system and the flow angle sensor.

The pressure system uses an ESP-32 differential transducer. This 32-port transducer is capable of automatic calibration and produces an analog multiplexed signal. The signal must be demultiplexed and filtered at 100 hertz (Hz) using a control system designed at SERI. Signals are then passed on to a pulse-code modulation (PCM) data acquisition system (DAS), which samples the analog signals at a frequency of 522 Hz. The transducer is mounted inside the blade near the 75% span. Tubes laminated into the blade skin transmit surface pressures to the transducer (Figure 1). Tube lengths run between 25 and 45 cm. Frequency-response measurements were made on the tubes. Results indicated less than 2% amplification of the pressure fluctuations for frequencies less than 50 Hz. The first "organ pipe" frequency was usually around 75 Hz. At this natural frequency, pressure amplifications were typically from 15% to 40%.

The frequency-response characteristics of this tube system were unacceptable for pressures fluctuating at high frequencies. To correct this distortion, an inverse transfer function (ITF) analytical technique was planned. Irwin et al. (4) describe this technique in detail. After analyzing some data, it became clear that this correction was not necessary for this pressure data because the spectral amplitude was negligible above 35 Hz. However, the correction proved useful for the flow angle sensor, which has a lower frequency response and significant amplification at 8-10 Hz, as will be discussed later.

Flow Angle Sensor

Because the main objective of these aerodynamic measurements was to compare wind tunnel data with rotating blade data, an accurate means of comparison was very important. The most direct and common measurement for comparing various data sets is AOA. This is a fairly easy measurement to make in the wind tunnel because the geometric angle was used. But on the rotor this is not the case. Local upwash effects, as well as induced velocities created by rotor wake

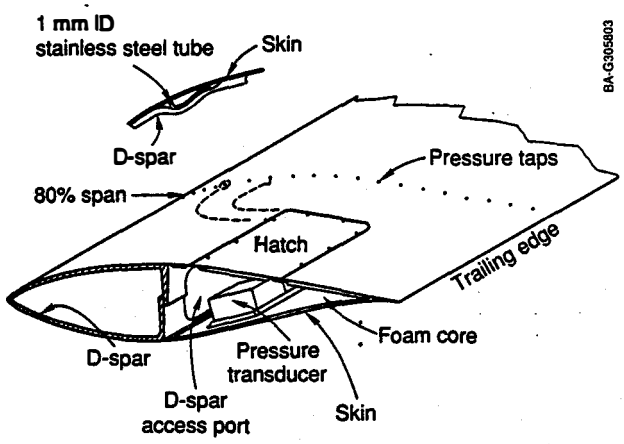

Figure 1. Layout of the pressure transducer on the blade.

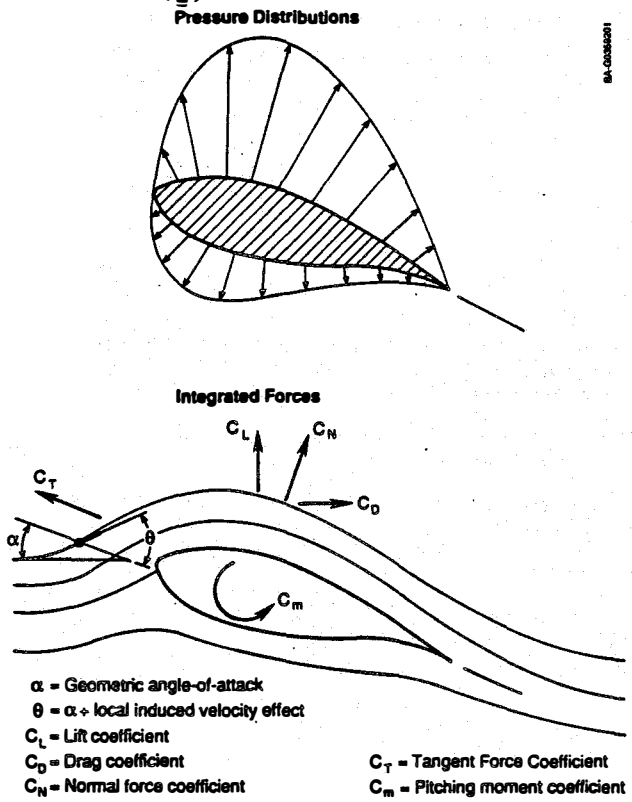

Figure 2. Local flow effects on a lifting airfoil.

expansions, distort the flow near the airfoil. Figure 2 shows typical streamlines under the influence of circulation-induced upwash. It was decided to use both analytical and experimental techniques in a "best effort" approach in accurately determining the correct AOA from measured local flow angles (LFA). The sensor used to obtain experimental measurements is described as follows.

Figure 3 shows the flow angle sensor that was developed by SERI for this test program. Lenschow (5) describes early development and testing of a similar sensor used in atmospheric flight testing. The sensor uses a very lightweight rigid flag, which aligns itself with the local flow. The flag angle is measured with a commercial rotary position sensor. The generated analog signal is recorded by the DAS. Flag angles can be measured within 0.1° accuracy. The sensor is mounted 0.8 chord lengths ahead of the leading edge on the 45.7-cm-chord blade. It was positioned at 86% of blade span (6% outboard of the pressure taps) to limit flow disturbances on the blade in front of the pressure taps. A total pressure probe was mounted at the tip of the sensor to record dynamic pressure measurements.

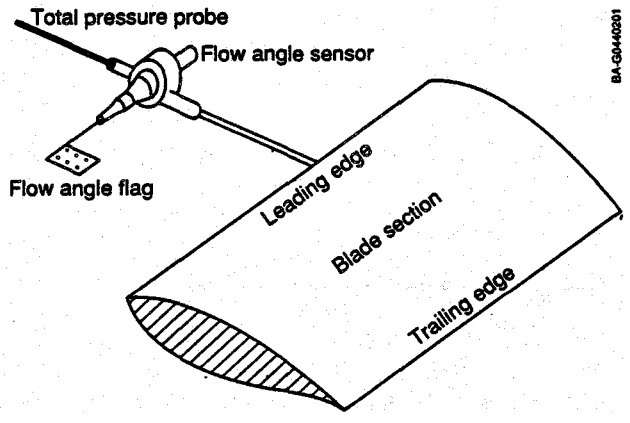

Figure 3. Layout of the flow angle sensor on the blade.

The accuracy of flow angle measurements and the relationship to the wind tunnel AOA were issues of concern. To investigate these issues, the sensor and probe were mounted on the wind tunnel model during testing. The effects of upwash, frequency response, and Reynolds number were determined.

Figure 4 shows the results of these tests. The dashed line in Figure 4 indicates a zero-correction line, or a condition where the flow angle sensor would measure the same angle as the geometric model angle during the wind tunnel testing. Triangles show data measured by the flow angle sensor. As can be seen, the upwash affect is important. At a geometric angle of 10°, the flow angle sensor indicates a 14° angle. The 4° discrepancy is due to the net effect of bound circulation and wake-induced flow. The solid line shows an analytical prediction of upwash effect. The Kutta-Joukowski Theorem was used to estimate the bound circulation, and the Biot-Savart Law was used to determine the local induced velocity. Induced velocities were vectorially added to the resultant inflow velocity to determine the corrected flow angle. The agreement is reasonable at low angles, where the flow is attached to the airfoil; however, as the angle increases and the flow separates, the agreement gets poor. Reynolds number effects were estimated to be insignificant for the steady-state wind tunnel tests. The wind tunnel data correction was used as the steady correction in field test data analysis.

To test the dynamic response of the flow angle sensor, the flag was deflected and released while the tunnel was running at various Reynolds numbers. The ring-down was recorded, from which a second-order system natural frequency and logarithmic damping ratio were determined. Figure 5 shows the results of ring-downs at Reynolds numbers equal to 1,000,000, along with the analytical approximations. Analytical results were approximated using measured frequencies and damping from the ring-down tests, plus a second-order differential equation. From the comparisons, it is clear that the flow angle sensor is well damped but not critically damped. Also, a second-order differential equation models the response well. The model shown, plus the ITF technique mentioned earlier, will be used in future data analyses to correct the frequency response, in both phase and magnitude, out to about 15 Hz.

This discussion addresses the issue of flow-angle-sensor dynamic characteristics. However, dynamic bound circulation changes could cause local flow field modifications that would alter the steady correction shown in Figure 4. These effects are unknown at this time. Future dynamic-stall wind tunnel tests will be attempted to address this issue. The flow angle sensor will be mounted on a model in the wind tunnel, while the model AOA is oscillated at representative frequencies. The effect of the dynamic flow field on upwash will be

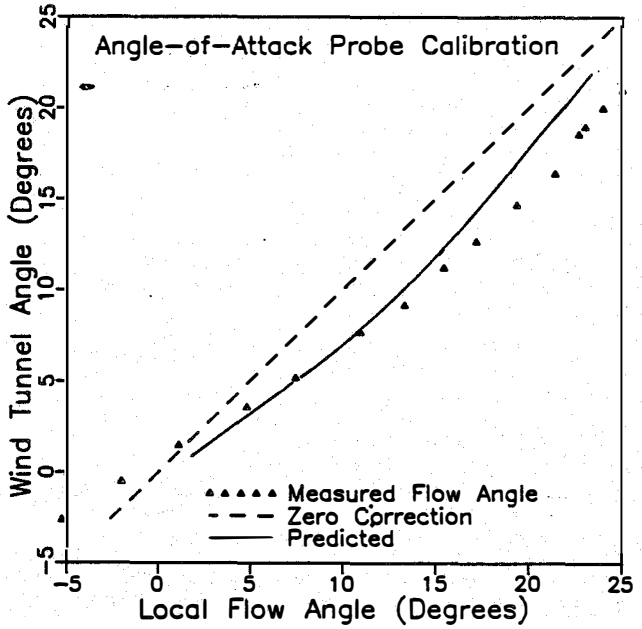

Figure 4. Wind tunnel calibration of the flow angle sensor

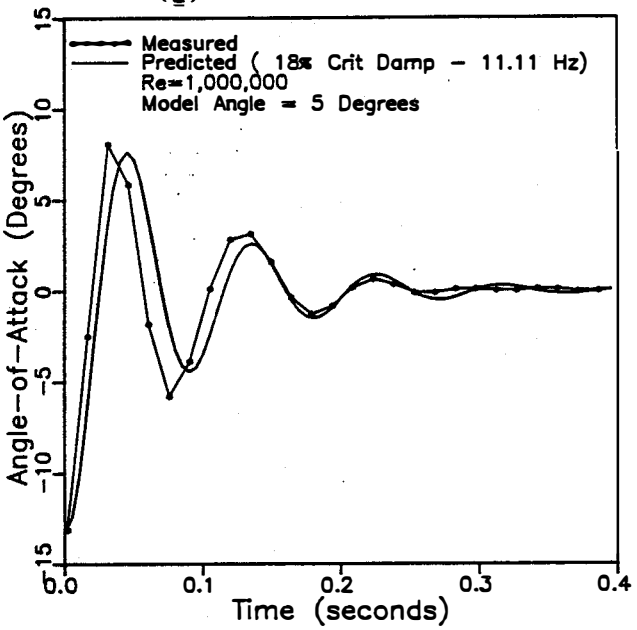

Figure 5. Dynamic response test of the flow angle sensor (Reynolds number = 1,000,000).

reflected in a comparison between geometric AOA and measured LFA.

Note that LFA data presented throughout this report are not corrected for either flow-angle-sensor dynamic characteristics or dynamic flow field effects. However, the flow angle sensor dynamic effects are estimated to be minimal on AOA variations less than 2 Hz because the sensor's natural frequency is approximately 10 Hz (8.3 times the rotor frequency). Also, the data are block-averaged from 522 to 10 Hz. This averaging should reduce the scatter due to dynamics of the flow angle sensor. Another fact that supports the assumption that dynamically induced errors in AOA measurements are small is that data scatter is small for low to moderate LFA. If the dynamic effects mentioned previously were playing a large roll, then we could expect to see significant scatter throughout the entire range of LFA. Yet scatter is only large at high LFA, where stall is present (as shown later in Figure 9). These results will be discussed in more detail in the following section.

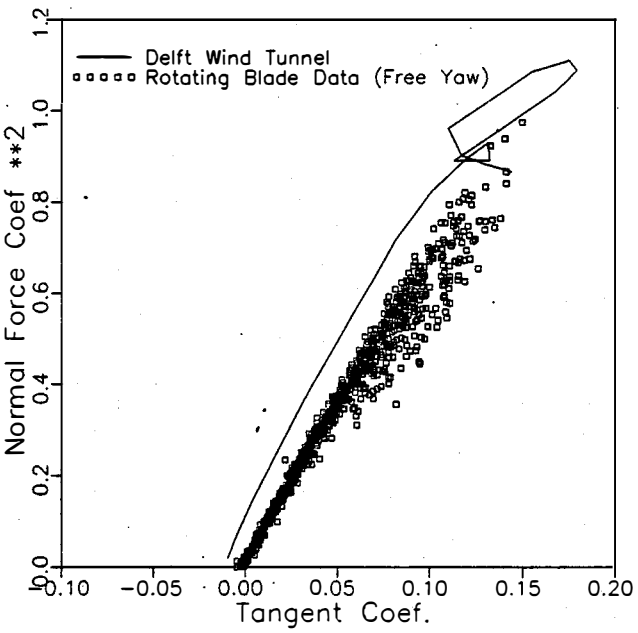

Figure 6. Linear aerodynamics test.

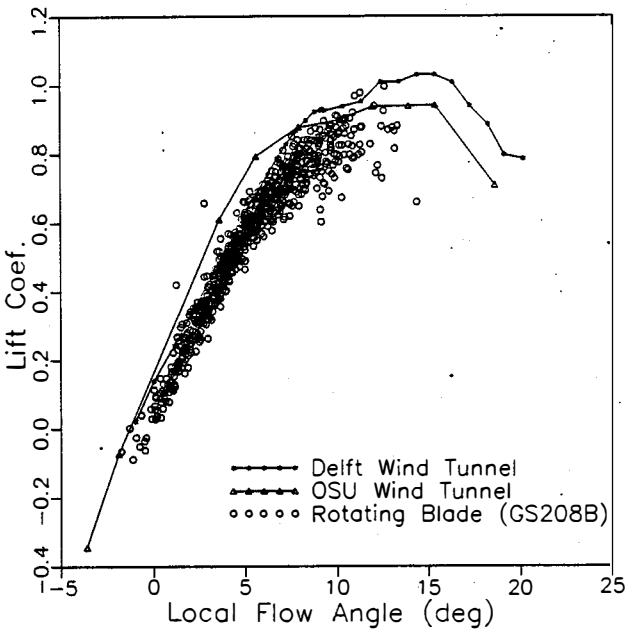

Figure 7. Comparison of rotating blade and wind tunnel data.

RESULTS

Data presented in Figures 6-10 were sampled at 522 Hz and were then block averaged to 10 Hz. Data in Figure 12 were block averaged to 20 Hz. The wind turbine was operated at a constant 12° pitch angle. Measured pressure distributions were normalized by dynamic pressure to get pressure coefficients along the airfoil. These coefficients were integrated around the airfoil to obtain Normal Force Coefficients (C_n), tangent coefficients (C_t), lift coefficients (C_l), pressure drag coefficients (C_{dp}), and pitching moment coefficients (C_m). Figure 2 shows these normalized coefficients and their respective orientations. The first test of valid data to be applied was a test of linearity. Using linear aerodynamics, it can easily be shown that plotting C_n^2 versus C_t will result in a straight line with slope equal to a plot of C_l versus AOA. This relationship is true only for AOA below stall angles. Figure 6 is a plot of rotating blade data compared with data from the Delft University of Technology (Netherlands) wind tunnel. The turbine was operating in free yaw, with wind

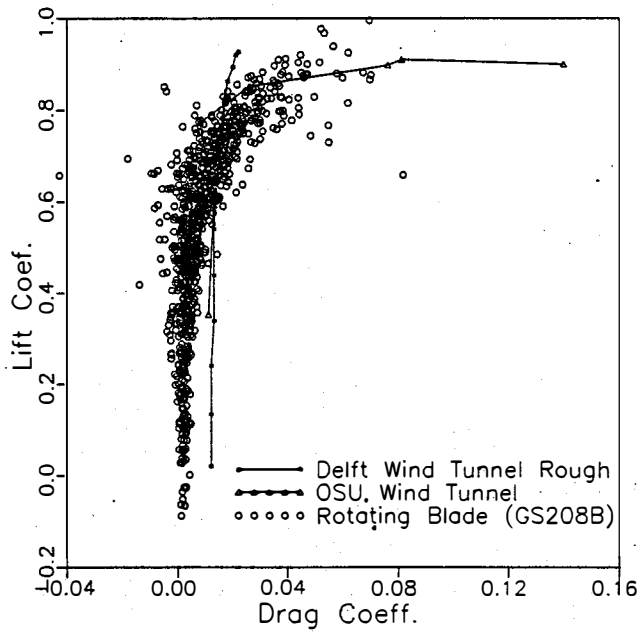

Figure 8. Comparison of drag data.

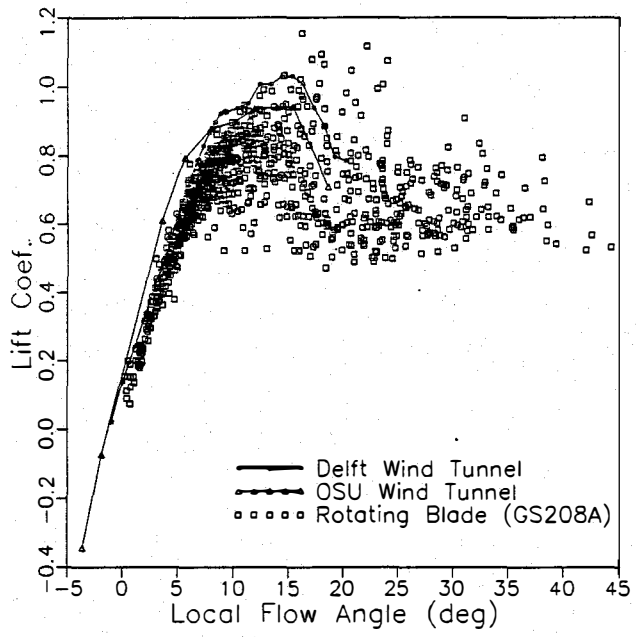

Figure 9. Lift characteristics at deep stall.

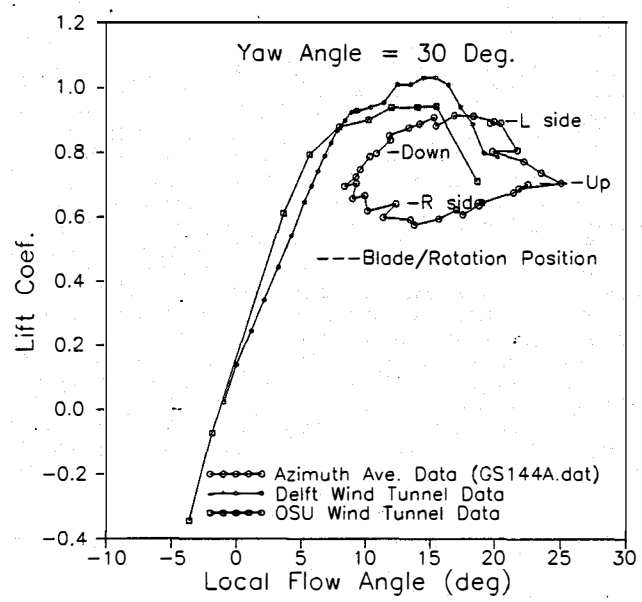

Figure 10. Azimuth-averaged lift data.

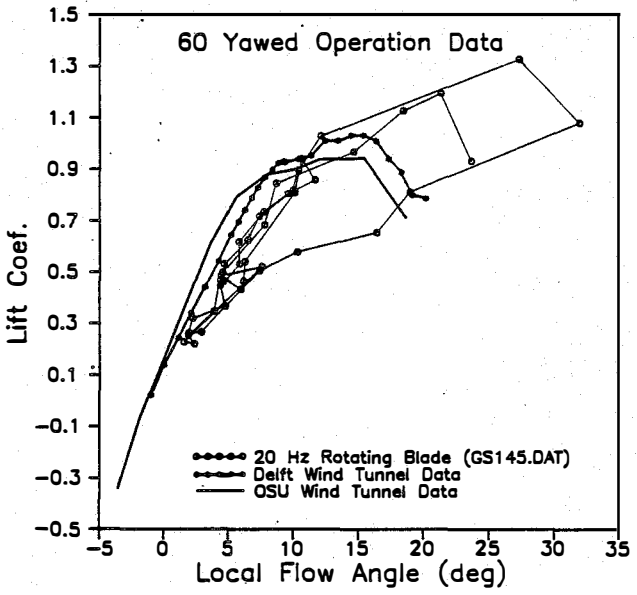

Figure 11. Dynamic stall during 60° yaw.

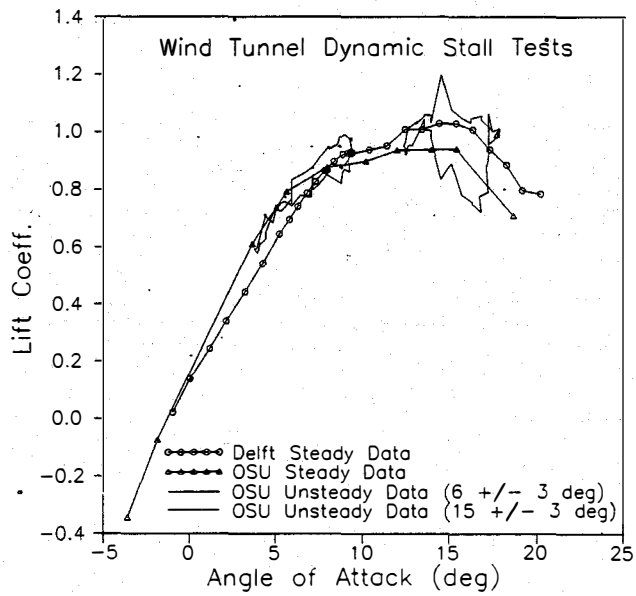

Figure 12. Wind tunnel dynamic stall tests.

speeds between 7 and 10 m/s. The offset between the two data sets is due to the method of calculating Delft C_n and C_t. These values were determined from measured values of AOA, C_l, and C_d. Delft C_d data included friction drag, causing the observed shift. Otherwise, the agreement is reasonably good, implying that this airfoil performs on a HAWT as it did in the wind tunnel for moderate AOA.

Next, C_l values from the rotating blade data were compared to wind tunnel data for the same operating conditions. Here, the measured LFA was corrected for steady upwash effects (as described earlier) before comparisons. Rotating blade data were chosen for "steady" conditions, where the wind speeds and AOA were moderate. Figure 7 shows this data compared with two sets of wind tunnel data--from Delft and from Ohio State University (OSU) in the United States. The data compare fairly well. There is approximately a 10% drop in the slope and evidence of a similar drop in C_{lmax} for rotating blade data. This is similar to the findings of Madsen et al. (1) for airfoils located outboard on the blade.

Using only pressure taps mounted on the blade, the pressure drag can be measured. This measure of drag will not account for skin friction drag, which implies that the minimum pressure drag will be zero if the flow over the airfoil is completely attached. The difference between C_{dpmin} and total drag measured in the wind tunnel is an estimate of the skin friction. Figure 8, which compares rotating blade data C_{dp} with wind tunnel data, shows this quite clearly. The figure also shows that rotating blade data C_{dp} is greater when C_l is greater than 0.8 for the Delft data. OSU data compare more favorably with rotating blade data. This implies that separation moves forward on the rotating airfoil sooner than shown by the two-dimensional data. This result is consistent with our findings of 10% lower C_{lmax}. It is also supported by comparisons of rotating blade data pressure distributions with wind tunnel pressure distributions (not presented in this report).

During high-wind operation, where the AOA is normally near stall, there is evidence of stall hysteresis. Figure 9 shows data for free-yaw operation in winds averaging 15 m/s and a reduced frequency of 0.05. Reduced frequency is defined as

$$K = \pi \times f \times c/v$$

where f is the rotor frequency, c is the chord, and v is the local inplane velocity. The noticeable scatter in the data for

AOA greater than 10° always exists in the rotating blade data. This can be attributed to unsteadiness in the inflow and stall hysteresis. There was no measurable stall hysteresis in the steady wind tunnel data. The maximum C_l measured during these high-AOA conditions was very infrequently greater than those measured in the wind tunnel, and it was usually less than wind tunnel C_{lmax} data. This is unlike dynamic stall, which is always associated with an increase in C_{lmax}. The size of the hysteresis loops ($C_{lmax} - C_{lmin}$) varies with the change of AOA. If any yaw angle exists, causing periodic variations in AOA, these loops become well-defined, once-per-revolution variations in C_l. Figure 10 shows azimuth-averaged data measured during 30° yawed operation. This plot clearly shows how lift reaches a maximum on the left (L) side of the rotation and a minimum on the right (R) side.

This lift hysteresis during yawed operation has serious implications on yaw-drive load and blade load for yaw-driven wind turbines. Hansen (6) has modeled this type of hysteresis using the Gormont Dynamic Stall Model and found that it can cause a doubling of mean yaw moments for this 10-m rotor.

Dynamic stall has also been observed during unsteady inflow and high-yaw-angle operation. This type of stall requires rapid AOA changes and results in an increase in C_{lmax} as well as hysteresis in the lift curve. Figure 11 shows an increase in C_{lmax} of 40% during operation at 60° of yaw angle and a reduced frequency (K) of 0.05. This was the worst case observed and was accompanied by a positive gust. The S809 airfoil was tested for dynamic stall at AOA peak-to-peak amplitudes of 6° and various mean values of AOA. Figure 12 shows the results of these tests. A 15% increase in C_{lmax} resulting from unsteady aerodynamics can be seen in these test results. However, this increase in C_{lmax} for the S809 airfoil was found to be less than increases in C_{lmax} for the NACA 23015 or the NACA 4415 airfoils under the same unsteady conditions (7). Therefore, it is possible that many of the wind turbines presently operating with the NACA airfoils could experience greater dynamic stall effects than those shown in Figure 11 for the S809.

FUTURE WORK

Stall behavior of wind turbines is complex, yet it must be understood if loads and performance are to be accurately predicted. The investigations of this report do not tell the complete story. For example, reference (1) suggests that pressure measurements at inboard spanwise stations might reveal different stall behavior. Stall behavior on rotating turbine blades is a three-dimensional phenomenon. Pressure measurements must be made at several spanwise stations to provide a complete understanding of the three-dimensional nature of this behavior. Flow-visualization data must be correlated with pressure measurements to understand the three-dimensional progression of separation on the blade. Analytical or semi-empirical models are needed to describe the physics of the process. SERI will continue work to resolve these important technical challenges.

CONCLUSIONS

At higher AOA, near and beyond stall, significant stall hysteresis is evident in the data. This hysteresis was greater than that measured in the wind tunnel. For large yaw angles, significant increases in C_{lmax} can accompany stall hysteresis, resulting in "dynamic stall." At low AOA, rotating blade data appear to experience a slight drop in lift curve slope and C_{lmax}. A method of measuring AOA was developed and tested that serves as a good correlation parameter to allow comparison with wind tunnel data.

ACKNOWLEDGMENTS

Many people have contributed to this research program. Dave Simms, Walt Musial, Mike Jenks, Bob Thresher, Al Eggers, Craig Hansen, Bob Akins, and Karl Danninger all made direct contributions that deserve recognition and thanks. Without the support of the U.S. Department of Energy, the program would not have been possible. Their foresight must be applauded.

REFERENCES

1. Madsen, H. A., Rasmussen, F., and Pedersen, T. F., 1988, *Aerodynamics of a Full-Scale HAWT Blade*, Riso National Laboratory, DK-4000, Roskilde, Denmark ECWEC '88.

2. Tangler, J. L., 1987, *Status of the Special-Purpose Airfoil Families*, SERI/TP-217-3264, Solar Energy Research Institute, Golden, Colorado.

3. Butterfield, C. P., 1989, "Aerodynamic Pressure and Flow-Visualization Measurement from a Rotating Wind Turbine Blade" SERI/TP-217-3433, Solar Energy Research Institute, Golden, Colorado.

4. Irwin, H. P. H. H., Cooper, K. R., and Hirard, R., 1979, "Correction of Distortion Effects Caused by Tubing Systems in Measurements of Fl tuating Pressures," Journal of Industrial Aerodynamics 5, pp. 93-107.

5. Lenschow, D. H., 1971, "Vanes for Sensing Incidence Angles of the Air from an Aircraft," D.H. Lenschow, Journal of Applied Meteorology, 10, (6), pp. 1339-1343.

6. Hansen, A. C. and Butterfield, C. P., 1989, "Yaw Loads and Motions of a Horizontal Axis Wind Turbine," Proceedings of the European Wind Energy Conference, Glasgow, Scotland, July 1989.

7. Unpublished results from dynamic stall tests performed at the Ohio State University wind tunnel.